AIAA JOURNAL
Vol. 47, No. 5, May 2009

Interfacial-Area Transport Equation at Reduced-Gravity Conditions

Takashi Hibiki*
Purdue University, West Lafayette, Indiana 47907-2017
Tatsuya Hazuku† and Tomoji Takamasa‡
Tokyo University of Marine Science and Technology, Tokyo 135-8533, Japan
and
Mamoru Ishii§
Purdue University, West Lafayette, Indiana 47907-2017

DOI: 10.2514/1.38208

The interfacial-area transport equation is of practical importance for two-phase flow analyses at reduced-gravity conditions. In view of this, the interfacial-area transport equation, which takes the gravity effect into account, is studied in detail. The constitutive equation for the sink term of the interfacial-area concentration due to wake entrainment has been developed by considering the body acceleration due to frictional pressure loss. A comparison of the newly developed interfacial-area transport equation with various experimental data taken at normal-gravity and microgravity conditions shows a satisfactory agreement. An example computation of the newly developed interfacial-area transport equation has been performed at various gravity conditions such as 0, 1.62, 3.71, and 9.80 m/s^2, which correspond to zero-gravity and the lunar, Martian, and Earth surface gravities, respectively. It has been revealed that the effect of the gravity on the interfacial-area transport in a two-phase flow system is more pronounced for low-liquid-flow and low-void-fraction conditions, whereas the gravity effect can be ignored for high-mixture-volumetric-flux conditions.

Nomenclature

A	=	cross-sectional area
a_i	=	interfacial-area concentration
C_A	=	coefficient
C_D	=	drag coefficient
C_P	=	coefficient
C_V	=	coefficient
C_0	=	distribution parameter
D	=	diameter of a pipe
D_b	=	bubble diameter
D_{Sm}	=	Sauter mean diameter
g	=	gravitational acceleration
g_N	=	normal gravitational acceleration
j	=	mixture volumetric flux
j_f	=	superficial liquid velocity
j_g	=	superficial gas velocity
K_B	=	constant
K_C	=	constant
M_F	=	frictional pressure gradient in the multiparticle system
N_{Re_f}	=	liquid Reynolds number
p	=	pressure
r_b	=	bubble radius
t	=	time
v_g	=	average center-of-volume velocity of the gas phase
v_{gj}	=	drift velocity
v_i	=	interfacial velocity
v_r	=	relative velocity
$\bar{v}_r$	=	difference between area-averaged mean velocities of phases
z	=	axial distance
α	=	void fraction
$\alpha_{B,\max}$	=	void fraction at maximum bubble-eddy packing
$\alpha_{C,\max}$	=	void fraction at maximum bubble packing
Γ_{RC}	=	adjustable coefficient
Γ_{TI}	=	adjustable coefficient
Γ_{WE}	=	adjustable coefficient
$\Delta\rho$	=	density difference between phases
ε	=	energy dissipation rate per unit mass
η_{ph}	=	rate of volume generated by nucleation source per unit mixture volume
ν_f	=	kinematic viscosity
ρ_f	=	liquid density
ρ_g	=	gas density
ρ_m	=	mixture density
σ	=	surface tension
Φ_B	=	source term due to bubble breakup
Φ_C	=	sink term due to bubble coalescence
Φ_j	=	sink or source terms due to bubble coalescence or breakup
Φ_{ph}	=	sink or source terms due to phase change
Φ_{RC}	=	sink term due to bubble coalescence induced by bubble random collision
Φ_{TI}	=	source term due to bubble breakup induced by turbulent impact
Φ_{WE}	=	sink term due to bubble coalescence induced by wake entrainment
$\langle\,\rangle$	=	area-averaged value
$\langle\langle\,\rangle\rangle$	=	void-fraction-weighted-averaged value
$\langle\langle\,\rangle\rangle_a$	=	interfacial-area concentration-weighted-averaged value

Subscript

0	=	test-section inlet

Received 22 April 2008; revision received 2 February 2009; accepted for publication 6 February 2009.

*Professor, School of Nuclear Engineering, 400 Central Drive.
†Associate Professor, Graduate School of Marine Science and Technology, Etchujima, Koto.
‡Dean, Graduate School of Marine Science and Technology, Etchujima, Koto.
§Walter H. Zinn Distinguished Professor, School of Nuclear Engineering, 400 Central Drive.

Introduction

THE basic structure of a two-phase flow can be characterized by two fundamental geometrical parameters. These are the void fraction and interfacial-area concentration. The void fraction expresses the phase distribution and is a required parameter for hydrodynamic and thermal design in various industrial processes. On the other hand, the interfacial area describes available area for the interfacial transfer of mass, momentum, and energy and is a required parameter for a two-fluid model formulation. Various transfer mechanisms between phases depend on the two-phase interfacial structures. Therefore, an accurate knowledge of these parameters is necessary for any two-phase flow analyses. This fact can be further substantiated with respect to two-phase flow formulation.

In view of the great importance to the thermal-hydraulic design of thermal-control systems at reduced-gravity conditions, a number of experimental researches have been performed for two-phase flows at reduced-gravity conditions by means of a drop tower and an aircraft [1–7]. The constitutive equations of the drift velocity at reduced-gravity conditions, which is a key parameter in the drift-flux model, have been successfully modeled by considering the body acceleration due to frictional pressure loss [8]. The constitutive equations of the distribution parameter in the drift-flux model at reduced-gravity conditions have been also developed based on extensive databases at reduced-gravity conditions [8].

On the other hand, there are very few established theoretical foundations to predict the interfacial-area concentration at reduced-gravity conditions. The concept of the interfacial-area transport equation has been proposed to provide the true dynamic nature of changes in the interfacial structure [9]. Continuous efforts to develop the interfacial-area transport equation have been made at normal-gravity conditions. However, there are very few attempts to develop the interfacial-area transport equation at reduced-gravity conditions.

From the viewpoint of the practical importance to the interfacial-area transport equation for two-phase flow analyses at reduced-gravity conditions, this study is focusing on the development of the interfacial-area transport equation, taking the gravity effect into account. First, this paper will briefly describe the basic concept of the interfacial-area transport equation developed at normal-gravity conditions. Next, to extend the interfacial-area transport equation at normal-gravity conditions to reduced-gravity conditions, the interfacial-area transport equation is modified by considering the body acceleration due to frictional pressure loss and is evaluated by data taken at normal-gravity and microgravity conditions. Finally, the interfacial-area transport equation is applied to various gravity conditions such as 0, 1.62, 3.71, and 9.80 m/s^2, which correspond to zero gravity and the lunar, Martian, and Earth surface gravities, respectively, and the effect of the gravity on the interfacial-area transport in two-phase flow systems is discussed.

Interfacial-Area Transport Equation

Formulation of Interfacial-Area Transport Equation

The interfacial-area transport equation can be formulated by considering the fluid particle number density transport equation to be analogous to Boltzmann's transport equation [9]. The general form of the three-dimensional interfacial-area transport equation is given by

$$\frac{\partial a_i}{\partial t} + \nabla \cdot (a_i \mathbf{v}_i) = \frac{2}{3}\left(\frac{a_i}{\alpha}\right)\left\{\frac{\partial \alpha}{\partial t} + \nabla \cdot (\alpha \mathbf{v}_g)\eta_{\mathrm{ph}}\right\} + \sum_j \Phi_j + \Phi_{\mathrm{ph}} \tag{1}$$

where a_i, t, $\mathbf{v}_i$, α, and $\mathbf{v}_g$ are, respectively, the interfacial-area concentration, time, interfacial velocity, void fraction, and average center-of-volume velocity of the gas phase. The first term on the right-hand side of Eq. (1) represents the sink or source term in the interfacial-area concentration due to void-fraction change. This term includes the rate of volume generated by nucleation source per unit mixture volume, η_{ph}. The terms Φ_j and Φ_{ph} represent the sink and source terms due to bubble coalescence and breakup and phase change, respectively. Under an adiabatic flow condition, the interfacial-area transport equation can be simplified to

$$\frac{\partial a_i}{\partial t} + \nabla \cdot (a_i \mathbf{v}_i) = \frac{2}{3}\left(\frac{a_i}{\alpha}\right)\left\{\frac{\partial \alpha}{\partial t} + \nabla \cdot (\alpha \mathbf{v}_g)\right\} + \sum_j \Phi_j = \frac{2}{3}\left(\frac{a_i}{\alpha}\right)\left\{\frac{\partial \alpha}{\partial t} + \nabla \cdot (\alpha \mathbf{v}_g)\right\} + \Phi_B - \Phi_C \tag{2}$$

where Φ_B and Φ_C are, respectively, the source term of the interfacial-area concentration due to bubble breakup and the sink term of the interfacial-area concentration due to bubble coalescence.

A one-dimensional form of the interfacial-area transport equation with relatively uniform distribution of flow parameters is approximated by (see Appendix A)

$$\frac{\partial \langle a_i \rangle}{\partial t} + \frac{\partial}{\partial z}(\langle a_i \rangle \langle\langle v_i \rangle\rangle_a) = \frac{2}{3}\left(\frac{\langle a_i \rangle}{\langle \alpha \rangle}\right)\left\{\frac{\partial \langle \alpha \rangle}{\partial t} + \frac{\partial}{\partial z}(\langle \alpha \rangle \langle\langle v_g \rangle\rangle)\right\} + \langle \Phi_B \rangle - \langle \Phi_C \rangle \tag{3}$$

where $\langle\,\rangle$, $\langle\langle\,\rangle\rangle_a$, and $\langle\langle\,\rangle\rangle$ are, respectively, the area-averaged, interfacial-area concentration-weighted-averaged, and void-fraction-weighted-averaged quantities. The flow direction is denoted by z. For a steady adiabatic flow condition, the interfacial-area transport equation can be further simplified to

$$\frac{d}{dz}(\langle a_i \rangle \langle\langle v_i \rangle\rangle_a) = \frac{2}{3}\left(\frac{\langle a_i \rangle}{\langle \alpha \rangle}\right)\frac{d}{dz}(\langle \alpha \rangle \langle\langle v_g \rangle\rangle) + \langle \Phi_B \rangle - \langle \Phi_C \rangle \tag{4}$$

For a steady adiabatic one-dimensional flow at an equilibrium state of bubble coalescence and breakup ($\langle \Phi_B \rangle - \langle \Phi_C \rangle = 0$), the interfacial-area transport equation is reduced to the most simplified form as

$$\frac{d}{dz}(\langle a_i \rangle \langle\langle v_i \rangle\rangle_a) = \frac{2}{3}\left(\frac{\langle a_i \rangle}{\langle \alpha \rangle}\right)\frac{d}{dz}(\langle \alpha \rangle \langle\langle v_g \rangle\rangle) \tag{5}$$

This most simplified interfacial-area transport equation clearly indicates that the interfacial-area concentration varies along the flow direction due to the bubble volume change by the pressure change, even in a steady adiabatic flow at equilibrium state of bubble coalescence and breakup.

Sink and Source Terms in Interfacial-Area Transport Equation

To complete the interfacial-area transport equation, constitutive relations for the sink and source terms appearing in the interfacial-area transport equation have to be developed. This can be achieved by modeling the bubble interaction mechanisms in a two-phase flow. Extensive work has been done to model the sink and source terms in the interfacial-area transport equation of vertical bubbly flows in pipes at normal-gravity conditions [9–12]. In a bubbly-flow regime, two major bubble-coalescence mechanisms are usually considered. They are bubble random collision induced by liquid turbulence and bubble collision due to wake entrainment. On the other hand, bubble breakup is considered to occur due to turbulent impact on bubbles. In what follows, bubble-coalescence and bubble-breakup models developed at normal-gravity conditions are briefly explained.

Bubble random motions are induced by liquid turbulence and bubbles collide in a random manner. Based on this modeled mechanism, the one-dimensional form of the bubble random-collision term Φ_{RC} is formulated by [9,10,12]

$$\langle \Phi_{\mathrm{RC}} \rangle = \frac{\Gamma_{\mathrm{RC}} \langle \alpha \rangle^2 \langle \varepsilon \rangle^{1/3}}{\langle D_b \rangle^{5/3}(\langle \alpha_{C,\max} \rangle - \langle \alpha \rangle)} \exp\left(-\frac{K_C \rho_f^{1/2} \langle D_b \rangle^{5/6} \langle \varepsilon \rangle^{1/3}}{\sigma^{1/2}}\right) \tag{6}$$

where Γ_{RC}, ε, D_b, $\alpha_{C,\max}$, K_C, ρ_f, and σ are, respectively, the adjustable coefficient, energy dissipation rate per unit mass, bubble diameter, void fraction at maximum bubble packing (0.74), constant (1.29 for air–water system [10]), liquid density, and surface tension.

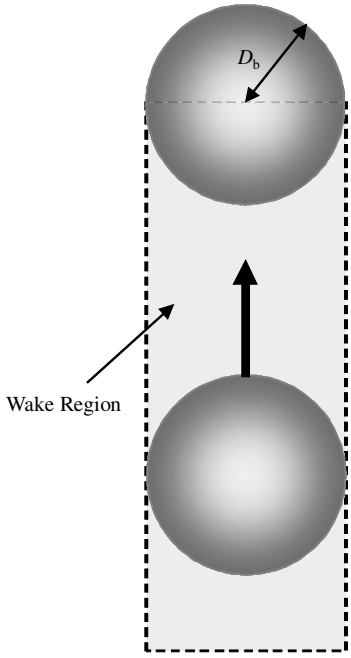

Fig. 1 Schematic diagram of wake-entrainment model [11].

When bubbles enter the wake region of a leading bubble, they will accelerate and may collide with the leading one (see Fig. 1). Based on this mechanism, the one-dimensional form of the bubble wake-entrainment term Φ_{WE} is formulated by [9,11]

$$\langle \Phi_{WE} \rangle = \Gamma_{WE} C_D^{1/3} \langle a_i \rangle^2 \langle v_r \rangle \exp\left(-\frac{K_C \rho_f^{1/2} \langle D_b \rangle^{5/6} \langle \varepsilon \rangle^{1/3}}{\sigma^{1/2}} \right) \quad (7)$$

where Γ_{WE}, C_D, and v_r are, respectively, the adjustable coefficient, drag coefficient, and relative velocity between phases. Note that $\langle \Phi_C \rangle = \langle \Phi_{RC} \rangle + \langle \Phi_{WE} \rangle$. When bubble diameter reaches about one-third of a channel diameter ($D_b/D \gtrsim 1/3$), bubble random motions are suppressed significantly by the presence of a channel wall and most of bubbles are in the wake region of preceding bubbles, resulting in wake entrainment as the dominant bubble-coalescence mechanism. In this case, it can be approximated that $\langle \Phi_C \rangle \approx \langle \Phi_{WE} \rangle$ [11]. A preliminary calculation supports the validity of this assumption in the test conditions listed in Tables 1 and 2. It should be also noted here that $\langle v_r \rangle$ is generally not equal to $\langle \langle v_g \rangle \rangle - \langle \langle v_f \rangle \rangle$. The approximate method to calculate $\langle v_r \rangle$ from $\langle \langle v_g \rangle \rangle$ and $\langle \langle v_f \rangle \rangle$ is given in Appendix B.

When turbulent eddies with sufficient energy and similar size to bubbles hit bubbles, bubbles are disintegrated into smaller bubbles. Based on this mechanism, the one-dimensional form of the turbulent-impact term Φ_{TI} is formulated by [9,10,12]

$$\langle \Phi_B \rangle = \langle \Phi_{TI} \rangle = \frac{\Gamma_{TI} \langle \alpha \rangle (1 - \langle \alpha \rangle) \langle \varepsilon \rangle^{1/3}}{\langle D_b \rangle^{5/3} (\langle \alpha_{B,max} \rangle - \langle \alpha \rangle)} \exp\left(-\frac{K_B \sigma}{\rho_f \langle D_b \rangle^{5/3} \langle \varepsilon \rangle^{2/3}} \right) \quad (8)$$

where Γ_{TI}, $\alpha_{B,max}$, and K_B are, respectively, the adjustable coefficient, void fraction at maximum bubble-eddy packing (0.74), and constant (1.59). When liquid velocity and void fraction are low, the turbulent-impact term is negligible [11]. A preliminary calculation supports the validity of this assumption in the test conditions listed in Tables 1 and 2. In Eqs. (6–8), terms expressed by exponential function indicate either bubble-coalescence or bubble-breakup efficiencies.

In the bubbly-flow regime, it can be approximated that $\langle \langle v_g \rangle \rangle \approx \langle \langle v_i \rangle \rangle_a$ [10,12]. For $D_b/D \gtrsim 1/3$, the steady one-dimensional interfacial-area transport equation at low liquid velocity is expressed as

$$\frac{d}{dz}(\langle a_i \rangle \langle \langle v_g \rangle \rangle) = \frac{2}{3} \left(\frac{\langle a_i \rangle}{\langle \alpha \rangle} \right) \frac{d}{dz}(\langle \alpha \rangle \langle \langle v_g \rangle \rangle) - \langle \Phi_{WE} \rangle \quad (9)$$

The wake-entrainment term can be evaluated solely by data taken in the conditions such as low liquid velocity and $D_b/D \gtrsim 1/3$.

Extension of Wake-Entrainment Model to Microgravity Condition

Equation (7) indicates a general form of the wake-entrainment term. In our previous work [14], we formulated the drag coefficient in a confined channel by taking into account the effect of a frictional

Table 1 Experimental conditions at normal-gravity conditions [13]

Flow parameters	Run 1	Run 2	Run 3	Run 4	Run 5
$\langle j_{g,0} \rangle$, m/s	0.018	0.015	0.064	0.065	0.057
$\langle j_f \rangle$, m/s	0.58	0.58	0.58	0.58	1.0
Gas injection method	A	B	A	B	A
Flow ratio[a]	68:32	86:14	68:32	86:14	71:29
C_{P0}, Pa	0.12351	0.12380	0.12435	0.12406	0.12605
C_{P1}, Pa	7.33549×10^{-6}	5.59328×10^{-6}	8.21246×10^{-6}	6.85111×10^{-6}	-5.93331×10^{-6}
C_{P2}, Pa	-2.73082×10^{-7}	-2.74533×10^{-7}	-2.96432×10^{-7}	-2.79385×10^{-7}	-2.47465×10^{-7}
C_{A0}	0.02117	0.01529	0.07307	0.06278	0.04374
C_{A1}	-1.73988×10^{-4}	-6.11150×10^{-5}	-1.92183×10^{-4}	-2.96728×10^{-4}	-2.06175×10^{-5}
C_{A2}	1.35002×10^{-6}	1.45565×10^{-6}	1.07026×10^{-6}	1.17274×10^{-6}	6.07901×10^{-7}
C_{V0}, m/s	0.86852	0.95004	0.87617	1.03160	1.31039
C_{V1}, m/s	-7.64381×10^{-5}	−0.00106	0.00357	0.00204	0.00189
$\langle a_{i,0} \rangle$, m^{-1}	64.64	42.89	120.0	103.3	82.07

[a]The ratio of flow in the inside pipe to flow in the annulus between the inside and outside pipes.

Table 2 Experimental conditions at microgravity conditions [6]

Flow parameters	Run 1	Run 2	Run 3	Run 4	Run 5	Run 6	Run 7
$\langle j_{g,0} \rangle$, m/s	0.015	0.0092	0.011	0.018	0.0083	0.015	0.022
$\langle j_f \rangle$, m/s	0.073	0.13	0.13	0.12	0.20	0.20	0.22
p, Pa	0.44	0.51	0.45	0.51	0.49	0.51	0.54
C_{A0}	0.0556	0.0268	0.01922	0.03154	0.00793	0.02078	0.02657
C_{A1}	6.60894×10^{-5}	-3.75154×10^{-5}	1.06059×10^{-4}	6.11385×10^{-4}	2.85692×10^{-4}	1.31201×10^{-4}	6.27265×10^{-4}
C_{A2}	-1.92663×10^{-6}	1.24256×10^{-7}	-2.24044×10^{-6}	-1.17271×10^{-5}	-3.75128×10^{-6}	-1.39212×10^{-6}	-9.14816×10^{-6}
$\langle a_{i,z/D=7} \rangle$, m^{-1}	90.0	64.0	46.4	65.8	30.7	53.7	72.7

pressure gradient due to a liquid flow:

$$C_D = \frac{8}{3}\frac{\langle r_b\rangle}{\rho_f\langle v_r\rangle^2}\{\Delta\rho g(1-\langle\alpha\rangle)+M_F\} = \frac{8\{\Delta\rho g(1-\langle\alpha\rangle)+M_F\}\langle\alpha\rangle}{\rho_f\langle v_r\rangle^2\langle a_i\rangle} \quad (10)$$

where $\langle r_b\rangle$ and g are, respectively, the area-averaged bubble radius expressed by $3\langle\alpha\rangle/\langle a_i\rangle$ and gravitational acceleration. Two-phase frictional pressure gradient M_F is given by

$$M_F = \left(-\frac{dp}{dz}\right)_F \quad (11)$$

where p is pressure. The validity of Eq. (10) has been verified by comparing the drift-flux model incorporated with Eq. (10) and experimental data taken at microgravity conditions [8].

Substituting Eq. (10) into Eq. (7) yields

$$\langle\Phi_{\mathrm{WE}}\rangle = \Gamma_{\mathrm{WE}}\left[\frac{8\{\Delta\rho g(1-\langle\alpha\rangle)+M_F\}}{\rho_f}\right]^{1/3}\langle\alpha\rangle^{1/3}\langle a_i\rangle^{5/3}\langle v_r\rangle^{1/3} \times \exp\left(-\frac{K_C\rho_f^{1/2}\langle D_b\rangle^{5/6}\langle\varepsilon\rangle^{1/3}}{\sigma^{1/2}}\right) \quad (12)$$

An expression for the energy dissipation rate per unit mass can be obtained from the mechanical energy balance on the assumption that the dissipation of turbulent energy in the flow is equal to its production [15]. The expression is extended by considering the effect of a frictional pressure gradient due to a liquid flow as

$$\langle\varepsilon\rangle = \left\{g+\frac{M_F}{\Delta\rho(1-\langle\alpha\rangle)}\right\}|\langle j_g\rangle|\exp(-0.0005839N_{Re_f}) + \frac{|\langle j\rangle|}{\rho_m}M_F\{1-\exp(-0.0005839N_{\mathrm{Re}_f})\} \quad (13)$$

where j_g and j are, respectively, the superficial gas velocity and mixture volumetric flux. Mixture density ρ_m and liquid Reynolds number N_{Re_f} are defined as Eqs. (14) and (15), respectively:

$$\rho_m = \rho_g\langle\alpha\rangle + \rho_f(1-\langle\alpha\rangle) \quad (14)$$

$$N_{Re_f} \equiv \frac{\langle j_f\rangle D}{\nu_f} \quad (15)$$

where ρ_g, j_f, D, and ν_f are, respectively, the gas density, superficial liquid velocity, channel diameter, and kinematic viscosity of the liquid phase.

The two-phase frictional pressure gradient M_F can be computed from the Lockhart–Martinelli method [16], which provides the estimation error in the order of ±30%. Because $\langle\Phi_{\mathrm{WE}}\rangle$ is approximately in proportion to $M_F^{1/3}$, the estimation error may not affect the estimation of $\langle\Phi_{\mathrm{WE}}\rangle$ significantly. For example, 30% estimation error in M_F approximately propagates 9% estimation error in $\langle\Phi_{\mathrm{WE}}\rangle$.

Experimental Data

Brief Description of Existing Experimental Data Characteristics

To evaluate the wake-entrainment term, we performed two kinds of experiments at normal and microgravity conditions. Interfacial-area transport data at normal-gravity conditions were obtained under the flow condition in which Eq. (9) holds: namely, low liquid velocity, $D_b/D \gtrsim 1/3$, and steady flow [11,13]. Γ_{WE} in Eq. (7) can be determined by the data.

Interfacial-area transport data at microgravity conditions were also obtained under the flow condition in which Eq. (9) holds [6]. Because this experiment was performed at 0.5 MPa to avoid any sudden gravitational head loss change at the instant of dropping a test section in a drop tower, the first term on the right-hand side of Eq. (9) is negligible. Thus, the data are ideal to verify the wake-entrainment model modified at microgravity conditions. The detailed explanations of these data will be given in what follows.

Experimental Data at Normal-Gravity Conditions

Axial changes of adiabatic air–water bubbly-flow parameters such as void fraction, interfacial-area concentration, and gas velocity were measured in a vertical 9-mm-diam and 945-mm-long pipe at 20°C and an atmospheric pressure under normal-gravity conditions [11,13]. A mixing chamber in the flow loop consisted of an air-injection nozzle placed in an inside pipe and the annulus between the inside and outside pipes to investigate the effect of the inlet bubble size on interfacial-area transport at the same gas and liquid flow rates. The details of the mixing chamber and flow-loop design can be found in our previous paper [13]. Measurements of flow parameters at 10 radial locations were performed by the stereo-imaging method at 6 axial locations of $z/D = 3$, 6, 12, 24, 57, and 91. One-dimensional flow parameters (namely, area-averaged flow parameters) were obtained by integrating the local flow parameters over the flow channel. To confirm the measurement accuracy, the imaging method was compared with the double-sensor-probe method in an experiment using a 25.4-mm-diam pipe [13,17]. The area-averaged interfacial-area concentrations measured by the imaging method agreed with those by the double-sensor-probe method within an average deviation of ±6.95% [17]. The measurement accuracy of the image-processing method was reported to be on the order of 10% [13]. A total of 5 data sets were acquired at flow conditions (inlet superficial gas velocity of 0.015–0.065 m/s and superficial liquid velocity of 0.58–1.0 m/s) listed in Table 1. The detailed experimental results are described in our previous paper [13].

To perform the interfacial-area transport calculation, axial values of pressure p, void fraction $\langle\alpha\rangle$, gas velocity $\langle\langle v_g\rangle\rangle$, and initial interfacial-area concentration $\langle a_{i,0}\rangle$ should be given by either constitutive relations or measured values. To evaluate the modeled wake-entrainment sink term, the flow parameters in the model should be given as accurately as possible. Therefore, the pressure, void fraction, and gas velocity are given here by the following fitting functions obtained from the measured flow parameters [11]:

$$p = C_{P0} + C_{P1}(z/D) + C_{P2}(z/D)^2 \quad (16)$$

$$\langle\alpha\rangle = C_{A0} + C_{A1}(z/D) + C_{A2}(z/D)^2 \quad (17)$$

$$\langle\langle v_g\rangle\rangle = C_{V0} + C_{V1}(z/D) \quad (18)$$

Coefficients in Eqs. (16–18) are listed in Table 1. Note that C_{P0}, C_{A0}, and C_{V0} correspond to the pressure, void fraction, and gas velocity at the test-section inlet, respectively.

Experimental Data at Microgravity Conditions

Axial changes of adiabatic nitrogen gas–water bubbly-flow parameters such as void fraction, interfacial-area concentration, and gas velocity were measured in a 9-mm-diam pipe at 20°C and about 0.5 MPa under microgravity conditions using an underground-drop shaft at the Japan Micro-Gravity Center (JAMIC) [6]. Among many drop shafts in the world, the one at the JAMIC, which has the longest free-fall depth (490 m), is one of the best facilities in view of a long duration of microgravity (about 10 s) and negligible residual gravity of 10^{-4}–$10^{-5}g_N$ ($1g_N = 9.8$ m/s^2, normal gravity).

A mixing chamber in the flow loop consisted of a double column made of an acrylic tube and a 7-mm-diam Teflon tube bubble generator with four holes of 0.6 mm diameter. The details of the mixing chamber and flow-loop design can be found in our previous paper [6]. Area-averaged flow parameters were measured by the image-processing method at 4 axial locations of $z/D = 7$, 30, 45, and 60. The measurement accuracy at microgravity conditions was similar to that at normal-gravity conditions. A total of 6 data sets were acquired at flow conditions (inlet superficial gas velocity of

0.0083–0.022 m/s and superficial liquid velocity of 0.073–0.22 m/s) listed in Table 2. The detailed experimental results are described in our previous paper [6].

Axial changes of pressure, void fraction, and gas velocity at microgravity conditions are given in a similar way to those of the normal-gravity experiment. Because the system pressure was maintained at about 0.5 MPa, the axial changes of pressure and void fraction were insignificant. The axial change of void fraction is calculated by Eq. (17) with coefficients given in Table 2. The gas velocity can be calculated by

$$\langle\langle v_g\rangle\rangle = \frac{\langle j_{g,0}\rangle}{\langle\alpha\rangle} \tag{19}$$

where $\langle j_{g,0}\rangle$ is the superficial gas velocity at the inlet. Because there are insufficient axial measurement locations due to limited space in the drop capsule, the interfacial-area concentrations at the inlet were not obtained by fitting the axial data change. Thus, the interfacial-area concentration measured at the first measuring station, $z/D = 7$, will be used as the initial value.

Results and Discussion

Evaluation of Wake-Entrainment Model Using Normal-Gravity Data

The sink and source terms of the interfacial-area concentration due to bubble random collision and turbulent impact are neglected in the interfacial-area transport calculation. These approximations are supported by a preliminary calculation of these terms and visual observation in the normal-gravity experiment. The axial change of interfacial-area concentration is computed from Eqs. (9) and (12). As can be seen from these equations, there is one adjustable coefficient, Γ_{WE}, in the interfacial-area transport equation. The value of Γ_{WE} is determined to be 0.232 using 5 data sets taken at normal-gravity conditions. In Eq. (12), the gravitational term is dominant over the frictional loss term at normal-gravity conditions, and Eq. (7) is usually used for computing the interfacial-area transport at normal-gravity conditions. However, because the adjustable coefficient Γ_{WE} determined by normal-gravity data will be used for computing the interfacial-area transport at microgravity conditions, the value of Γ_{WE} should be determined using the exact form of the wake-entrainment term [Eq. (12)].

Figure 2 compares the computed axial changes of interfacial-area concentrations with the measured ones for all 5 data sets. Figures 2a and 2b depict the comparisons for the data taken by injection methods A and B, respectively. Open symbols and lines indicate the measured and computed interfacial-area concentrations, respectively. Figure 3 shows the contribution of each mechanism to interfacial-area concentration change for two cases as typical examples of the data taken by injection methods A and B. Open symbols and solid lines indicate measured and computed interfacial-area concentration changes from the inlet interfacial-area concentration, $\langle a_i\rangle - \langle a_{i,0}\rangle$ respectively. Broken and dotted lines are, respectively, the interfacial-area concentration changes due to void-fraction change and wake entrainment.

There are essentially two mechanisms that contribute to axial interfacial-area concentration change due to void-fraction change along the flow direction. These mechanisms are bubble expansion due to pressure reduction along the flow direction and void distribution change along the flow direction. The bubble expansion

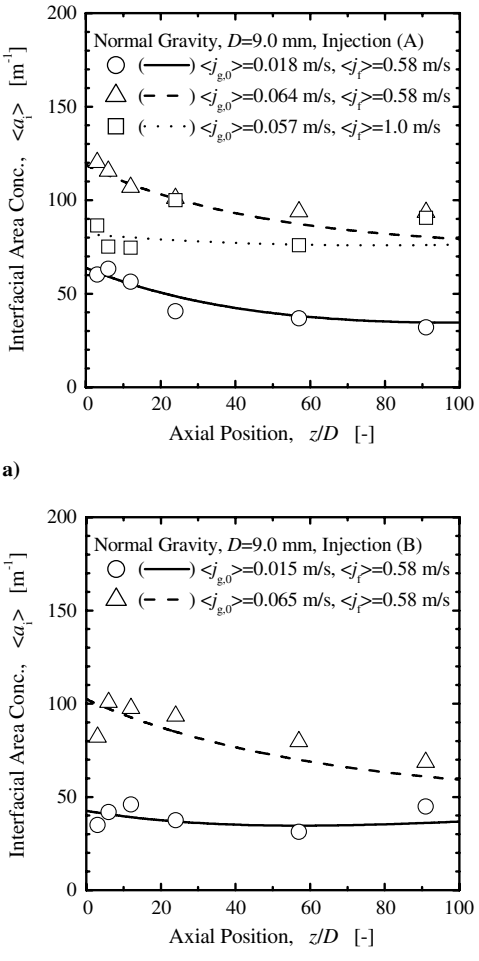

Fig. 2 Comparison of interfacial-area transport equation with measured interfacial-area concentrations at normal-gravity conditions: a) injection method A and b) injection method B.

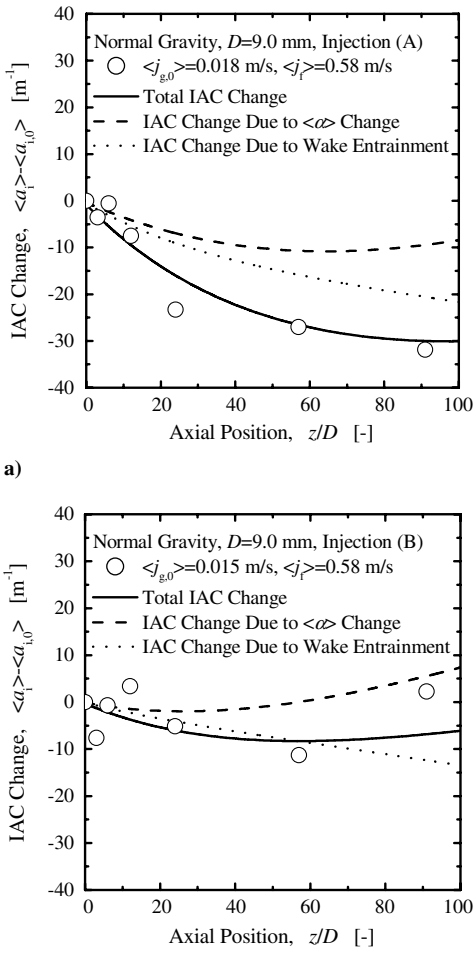

Fig. 3 Contributions of bubble coalescence and void transport to interfacial-area transport at normal-gravity conditions: a) injection method A ($\langle j_g\rangle = 0.018$ m/s and $\langle j_f\rangle = 0.58$ m/s) and b) injection method B ($\langle j_g\rangle = 0.015$ m/s and $\langle j_f\rangle = 0.58$ m/s); IAC denotes interfacial area concentration.

has a positive impact to increase the void fraction along the flow direction. Because the liquid velocity is relatively low, the void fraction increases between $z/D = 0$ and 91 due to pressure reduction being about 8% at maximum. As shown in the following drift-flux model [18], the void fraction is also changed by how the void distribution changes along the flow direction:

$$\langle \alpha \rangle = \frac{\langle j_g \rangle}{C_0 \langle j \rangle + \langle \langle v_{gj} \rangle \rangle} \tag{20}$$

where C_0 and v_{gj} are, respectively, the distribution parameter and drift velocity. The changes in void distribution from wall-peaked to core-peaked distributions increase the distribution parameter, resulting in the decreased void fraction. In an adiabatic bubbly flow, the maximum of void-fraction change due to void distribution change is generally 30% at bubbly-to-slug flow transition along a test section that is a few meters long. In the current database, this effect was negligibly small because local data did not show significant profile changes [6]. As shown in Fig. 3, the axial interfacial-area concentration change due to void-fraction change along the flow direction is insignificant for these cases.

The bubble coalescence due to wake entrainment decreases the interfacial-area concentration. As shown in Fig. 3a, the wake-entrainment effect enhances the axial decrease of the interfacial-area concentration. Figure 3b shows that the decrease of the interfacial-area concentration due to wake entrainment is countered by the increase of the interfacial-area concentration due to void-fraction increase along the flow direction, resulting in insignificant axial change of total interfacial-area concentration.

Figures 2 and 3 verify the validity of the interfacial-area transport equation with modeled wake-entrainment term [Eq. (12)] within the experimental conditions such as $0.015\ \text{m/s} \le \langle j_{g,0} \rangle \le 0.065\ \text{m/s}$ and $0.58\ \text{m/s} \le \langle j_f \rangle \le 1.0\ \text{m/s}$. The averaged prediction errors of the interfacial-area transport equation for all 30 points (6 axial locations times 5 flow conditions) and for 5 data points at $z/D = 91$ are ± 8.67 and $\pm 14.0\%$, respectively.

Evaluation of Wake-Entrainment Model Using Microgravity Data

The sink and source terms of the interfacial-area concentration due to bubble random collision and turbulent impact are neglected in the interfacial-area transport calculation. These approximations are supported by a preliminary calculation of these terms and visual observation in the microgravity experiment. The axial change of interfacial-area concentration is computed from Eqs. (9) and (12), with $\Gamma_{WE}(=0.232)$ determined based on normal-gravity data. Note that the first term in Eq. (9) is negligibly small due to relatively high system pressure ($p = 0.5$ MPa). If the contribution of body acceleration due to frictional pressure loss to relative velocity and drag coefficient is not considered, the wake-entrainment term is also computed to be zero, which means that the interfacial-area concentration should be constant along the flow direction.

Figure 4 compares the computed axial changes of interfacial-area concentrations with the measured ones for all 7 data sets. Figures 4a–4c depict the comparisons for the data taken at $\langle j_f \rangle = 0.073$, 0.13, and 0.21 m/s, respectively. Open symbols and lines indicate the measured and computed interfacial-area concentrations, respectively. The experimental data show the decrease trend of the interfacial-area concentration along the flow direction. Thus, bubble coalescence at microgravity conditions is experimentally confirmed. The interfacial-area concentrations computed with the wake-entrainment term [Eq. (12)] agree with the measured interfacial-area

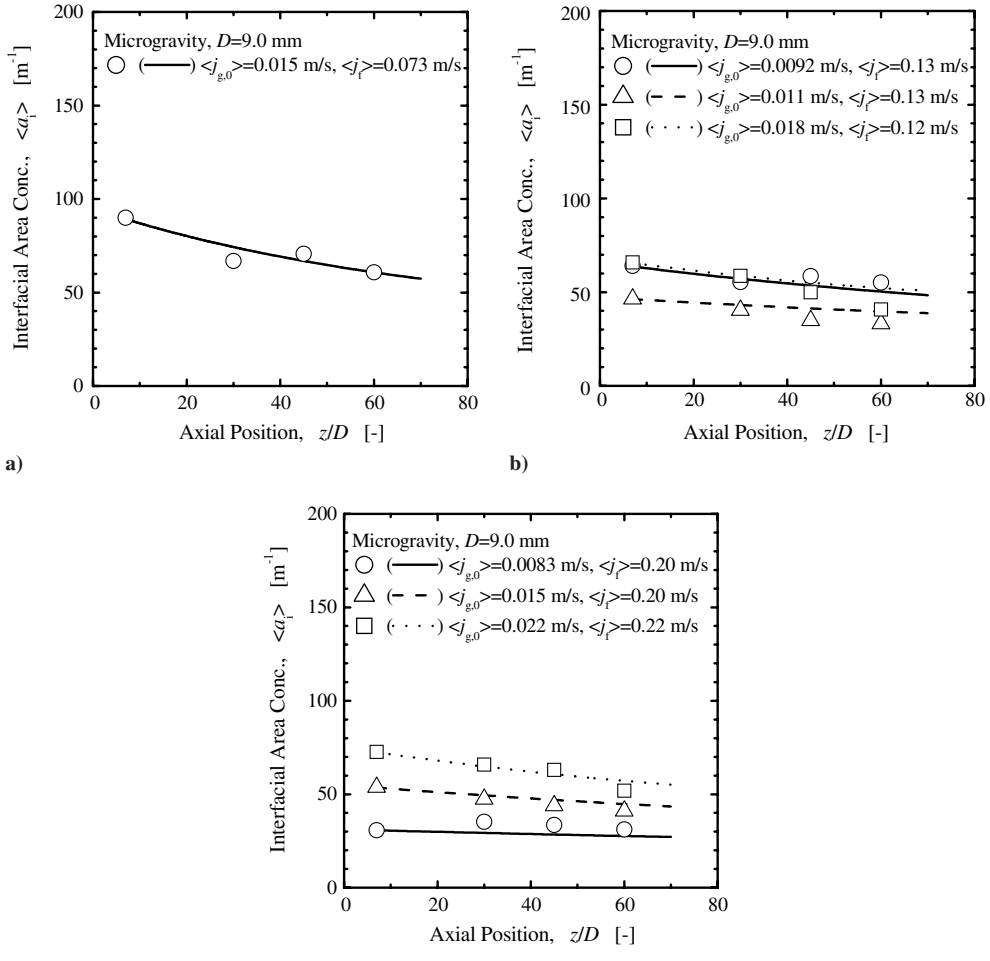

Fig. 4 Comparison of interfacial-area transport equation with measured interfacial-area concentrations at microgravity conditions: a) $\langle j_f \rangle = 0.073$ m/s, b) $\langle j_f \rangle = 0.13$ m/s, and c) $\langle j_f \rangle = 0.21$ m/s.

concentrations very well. This result indicates that body acceleration due to frictional pressure loss induces the wake entrainment, even at microgravity conditions.

Figure 4 verifies the validity of the interfacial-area transport equation with modeled wake-entrainment term within the experimental conditions of $0.0083\ \text{m/s} \leq \langle j_{g,0} \rangle \leq 0.022\ \text{m/s}$ and $0.073\ \text{m/s} \leq \langle j_f \rangle \leq 0.22\ \text{m/s}$. The averaged prediction errors of the interfacial-area transport equation for all 21 points (3 axial locations times 7 flow conditions) and for 7 data points at $z/D = 60$ are ± 7.29 and $\pm 12.6\%$, respectively.

Example Computations of Interfacial Area Transport Equation at Various Gravity Conditions

To examine the effect of the gravity level on the interfacial-area transport in two-phase flow systems, example computations using the developed interfacial-area transport equation are performed at various gravity levels. Major assumptions for these computations are 1) air–water system at 0.5 MPa; 2) uniform void distribution over the flow channel; 3) negligible drift velocity; 4) $\langle D_{\text{Sm},0} \rangle = 3$ mm, where $\langle D_{\text{Sm},0} \rangle$ is the area-averaged bubble Sauter mean diameter at the inlet; and 5) neglected bubble coalescence due to random collision and bubble breakup due to turbulent impact to evaluate the effect of gravity level on the wake-entrainment term only. Under these assumptions, no axial interfacial-area concentration changes occur if the body acceleration due to frictional pressure drop is not considered in the wake-entrainment term.

Figure 5 shows the computed axial change of the interfacial-area concentration at various gravity levels. The values of the interfacial-area concentration is normalized by inlet interfacial-area concentration, $\langle a_{i,0} \rangle$. The flow conditions for Figs. 5a–5d are $\langle \alpha_0 \rangle = 0.05$ and $\langle j_f \rangle = 0.5$ m/s, $\langle \alpha_0 \rangle = 0.2$ and $\langle j_f \rangle = 0.5$ m/s, $\langle \alpha_0 \rangle = 0.05$ and $\langle j_f \rangle = 2.0$ m/s, and $\langle \alpha_0 \rangle = 0.2$ and $\langle j_f \rangle = 2.0$ m/s, respectively. Solid, broken, dotted, and chain lines indicate the computed results for $0 - g_N$ (0.00 m/s^2), $0.165 - g_N$ (1.62 m/s^2), $0.379 - g_N$ (3.71 m/s^2), and $1 - g_N$ (9.80 m/s^2), corresponding to zero gravity and the lunar, Martian, and Earth surface gravities, respectively.

The comparison of Figs. 5a and 5b indicates that the increase in void fraction enhances the bubble coalescence, and the decrease in the interfacial-area concentration at $z/D = 100$ reaches about 50 and 70% for $\langle \alpha_0 \rangle = 0.05$ and 0.2, respectively. The effect of the gravity level on the interfacial-area concentration at $z/D = 100$ is less than 20 and 10% for $\langle \alpha_0 \rangle = 0.05$ and 0.2, respectively. This means that the bubble coalescence due to wake entrainment at microgravity conditions should be properly considered.

Figures 5c and 5d indicate insignificant axial change of the interfacial-area concentration at $\langle j_f \rangle = 2.0$ m/s on the order of 10 to 15%. The main reasons are 1) reduced residence time of two-phase flow for higher $\langle j_f \rangle$, resulting in reduced bubble coalescence, and 2) reduced bubble-coalescence efficiency for higher $\langle j_f \rangle$, resulting in suppressed bubble coalescence. One of the important findings is that the wake-entrainment term at a zero-gravity condition cannot be neglected because of the body acceleration due to frictional pressure loss.

Application of Developed Interfacial Area Transport Equation to General Bubbly-Flow Problems

In this study, the interfacial-area sink term due to wake entrainment [Eq. (12)] has been extended to reduced-gravity conditions and validated using the microgravity data obtained in the well-

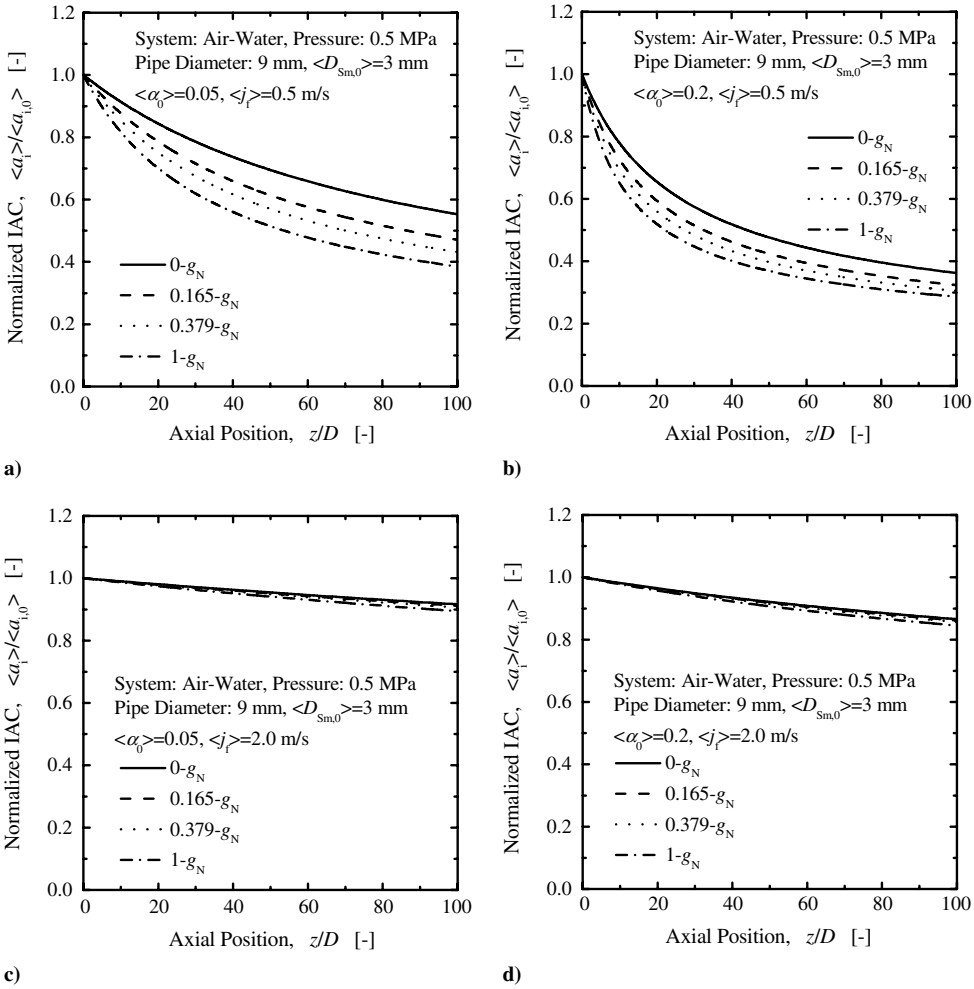

Fig. 5 Example computations of interfacial-area transport equation at various gravity levels: a) $\langle \alpha_0 \rangle = 0.05$ and $\langle j_f \rangle = 0.5$ m/s, b) $\langle \alpha_0 \rangle = 0.2$ and $\langle j_f \rangle = 0.5$ m/s, c) $\langle \alpha_0 \rangle = 0.05$ and $\langle j_f \rangle = 2.0$ m/s, and d) $\langle \alpha_0 \rangle = 0.2$ and $\langle j_f \rangle = 2.0$ m/s.

designed experimental conditions in which the interfacial-area sink term due to random collision [Eq. (6)] and the interfacial-area source term due to turbulent impact [Eq. (8)] can be neglected because of $D_b/D \gtrsim 1/3$ and low liquid velocity, respectively. To apply the interfacial-area transport equation to general bubbly-flow problems (higher liquid velocity and $D_b/D \lesssim 1/3$), the random-collision and turbulent-impact terms should be also implemented in the interfacial-area transport equation (2). Because the random-collision and turbulent-impact terms have no gravitational dependency, they may be applicable at reduced-gravity conditions. The random-collision and turbulent-impact terms have been experimentally validated in vertically upward bubbly-flow systems with the ranges of $0.262 \text{ m/s} \leq \langle j_f \rangle \leq 5.00 \text{ m/s}$, $0.0130 \leq \langle \alpha \rangle \leq 0.442$, and $25.4 \text{ mm} \leq D \leq 50.8 \text{ mm}$ at normal-gravity conditions [10]. Note that the coefficient K_C in Eqs. (6) and (12) may be dependent on physical properties.

Conclusions

The interfacial-area transport equation is of practical importance for two-phase flow analyses at reduced-gravity conditions. In view of this, the interfacial-area transport equation, which takes the gravity effect into account, was studied in detail. The obtained results are as follows:

1) The interfacial-area transport equation, which takes the gravity effect into account, has been developed, and the constitutive equation for the sink term of the interfacial-area concentration due to wake entrainment has been formulated by considering the body acceleration due to frictional pressure loss.

2) A comparison of the newly developed interfacial-area transport equation with experimental data taken at normal-gravity and microgravity conditions shows satisfactory agreement.

3) Example computations of the newly developed interfacial-area transport equation have been performed at various gravity conditions such as 0, 1.62, 3.71, and 9.80 m/s^2, corresponding to zero gravity and the lunar, Martian, and Earth surface gravities, respectively. It has been revealed that the effect of the gravity on the interfacial-area transport in a two-phase flow system is more pronounced at low-liquid-flow-rate and low-void-fraction conditions, whereas the gravity effect can be ignored at high-mixture-volumetric-flux conditions.

In this study, the wake-entrainment term has been verified by well-designed experiments using a relatively-small-diameter pipe. As the pipe diameter and liquid velocity increase, bubble coalescence due to random collision induced by liquid turbulence and bubble breakup due to turbulent impact may play an important role in the interfacial-area transport. As can be seen from Eqs. (6) and (8), these terms are insensitive to gravity level. Thus, it is expected that these equations may be applied to reduced-gravity conditions with reasonable accuracy. Further experimental works at reduced-gravity conditions are recommended to verify the applicability of Eqs. (6) and (8) to reduced-gravity conditions.

Appendix A: Covariance Due to Area-Averaging

Equation (3) is applicable to relatively uniform distribution of flow parameters over a flow channel. The exact mathematical expressions for the area-averaged source and sink terms would involve many covariances that may further complicate the one-dimensional problem. In the subcooled boiling-flow case, in which a very sharp void peak appears near a heated surface, the bubble-layer thickness model was developed to treat the flow parameter distribution in two regions (namely, the bubble-layer region and liquid single-phase flow region) to avoid any covariance [19]. In one-dimensional nuclear reactor thermal-hydraulics codes, the covariance terms in transport equations are usually neglected for simplicity. This simplified approach is adopted in this study. Thus, the empirical coefficient Γ_{WE} includes some covariance effects due to this simplification.

Appendix B: Area-Averaged Relative Velocity

The area-averaged local relative velocity $\langle v_r \rangle$ defined by Eq. (B1) should be used in the computation of the wake-entrainment term:

$$\langle v_r \rangle \equiv \frac{1}{A} \int v_r \mathrm{d}A \tag{B1}$$

where A is the flow channel area. In general, the area-averaged local relative velocity, which is difficult to obtain from operating conditions, is different from the difference between the area-averaged mean velocities of phases given by

$$\bar{v}_r \equiv \langle \langle v_g \rangle \rangle - \langle \langle v_f \rangle \rangle \tag{B2}$$

Based on the drift-flux model formulation, Ishii and Mishima [20] showed that the approximate expression for $\langle v_r \rangle$ is given by

$$\langle v_r \rangle \simeq \frac{1 - C_0 \langle \alpha \rangle}{1 - \langle \alpha \rangle} \langle \langle v_g \rangle \rangle - C_0 \langle \langle v_f \rangle \rangle \tag{B3}$$

for bubbly, slug, and churn turbulent flow. The distribution parameters at normal-gravity and microgravity conditions are estimated by Eq. (B4) [21] and Eq. (B5) [8], respectively:

$$C_0 = \frac{\langle \langle v_g \rangle \rangle - \sqrt{2}(\Delta \rho g \sigma / \rho_f^2)^{1/4}(1 - \langle \alpha \rangle)}{\langle \alpha \rangle \langle \langle v_g \rangle \rangle - (1 - \langle \alpha \rangle) \langle \langle v_f \rangle \rangle} \tag{B4}$$

$$\begin{aligned} C_0 = {} & 2.0 \exp(-0.000584 N_{Re_f}) + 1.0\{1 - \exp(-0.000584 N_{Re_f})\} \\ & - [2.0 \exp(-0.000584 N_{Re_f}) + 1.0\{1 - \exp(-0.000584 N_{Re_f})\} \\ & - 1] \sqrt{\frac{\rho_g}{\rho_f}} \end{aligned} \tag{B5}$$

Because $\langle \Phi_{\text{WE}} \rangle \propto \langle v_r \rangle^{1/3}$, the estimation error of $\langle v_r \rangle$ may not affect the estimation of $\langle \Phi_{\text{WE}} \rangle$. For example, 20 and 50% estimation errors in $\langle v_r \rangle$ propagate 6 and 14% estimation errors in $\langle \Phi_{\text{WE}} \rangle$.

Acknowledgments

Part of this work was supported by the Grant-in-Aid for Scientific Research from the Japan Science Forum. The authors would like to express their sincere appreciation to Yuriko Ohkubo (Tokyo University of Marine Science and Technology) for her help on this project.

References

[1] Colin, C., Fabre, J., and Dukler, A. E., "Gas-Liquid Flow at Microgravity Conditions—1: Dispersed Bubble and Slug Flow," *International Journal of Multiphase Flow*, Vol. 17, No. 4, 1991, pp. 533–544. doi:10.1016/0301-9322(91)90048-8

[2] Bousman, W. S., "Studies of Two-Phase Gas-Liquid Flow in Microgravity," NASA CR-195434, February, 1995.

[3] Fujii, T., Asano, H., Nakazawa, T., and Yamada, H., "Flow Characteristics of Gas-Liquid Two-Phase Flow Under Microgravity Condition," *Proceedings of the 2nd International Conference on Multiphase Flow '95*, Japanese Society for Multiphase Flow, Osaka, Japan, Apr. 1995, pp. P6-1–P6-5.

[4] Elkow, K. J., and Rezkallah, K. S., "Void Fraction Measurements in Gas-Liquid Flows Under 1-g and μ-g Conditions Using Capacitance Sensors," *International Journal of Multiphase Flow*, Vol. 23, No. 5, 1997, pp. 815–829. doi:10.1016/S0301-9322(97)00020-7

[5] Takamasa, T., Hazuku, T., Fukamachi, N., Tamura, N., Hibiki, T., and Ishii, M., "Effect of Gravity on Axial Development of Bubbly Flow at Low Liquid Reynolds Number," *Experiments in Fluids*, Vol. 37, No. 5, 2004, pp. 631–644. doi:10.1007/s00348-004-0844-9

[6] Takamasa, T., Iguchi, T., Hazuku, T., Hibiki, T., and Ishii, M., "Interfacial Area Transport of Bubbly Flow Under Microgravity Environment," *International Journal of Multiphase Flow*, Vol. 29,

No. 2, 2003, pp. 291–304.
doi:10.1016/S0301-9322(02)00129-5

[7] Choi, B., Fujii, T., Asano, H., and Sugimoto, K., "A Study of the Flow Characteristics in Air–Water Two-Phase Flow Under Microgravity (Results of Flight Experiments)," *JSME International Journal, Series B (Fluids and Thermal Engineering)*, Vol. 46, No. 2, 2003, pp. 262–269. doi:10.1299/jsmeb.46.262

[8] Hibiki, T., Takamasa, T., Ishii, M., and Gabriel, K. S., "One-Dimensional Drift-flux Model at Reduced Gravity Conditions," *AIAA Journal*, Vol. 44, No. 7, 2006, pp. 1635–1642. doi:10.2514/1.13159

[9] Ishii, M., and Hibiki, T., *Thermo-Fluid Dynamics of Two-Phase Flow*, Springer, New York, 2006.

[10] Hibiki, T., and Ishii, M., "One-group Interfacial Area Transport of Bubbly Flows in Vertical Round Tubes," *International Journal of Heat and Mass Transfer*, Vol. 43, No. 15, 2000, pp. 2711–2726. doi:10.1016/S0017-9310(99)00325-7

[11] Hibiki, T., Takamasa, T., and Ishii, M., "Interfacial Area Transport of Bubbly Flow in a Small Diameter Pipe," *Journal of Nuclear Science and Technology*, Vol. 38, No. 8, 2001, pp. 614–620.

[12] Hibiki, T., and Ishii, M., "Development of One-Group Interfacial Area Transport Equation in Bubbly Flow Systems," *International Journal of Heat and Mass Transfer*, Vol. 45, No. 11, 2002, pp. 2351–2372. doi:10.1016/S0017-9310(01)00327-1

[13] Takamasa, T., Goto, T., Hibiki, T., and Ishii, M., "Experimental Study of Interfacial Area Transport of Bubbly Flow in Small-Diameter Tube," *International Journal of Multiphase Flow*, Vol. 29, No. 3, 2003, pp. 395–409. doi:10.1016/S0301-9322(02)00167-2

[14] Hibiki, T., and Ishii, M., "One-dimensional Drift-flux Model and Constitutive Equations for Relative Motion Between Phases in Various Two-Phase Flow Regimes," *International Journal of Heat and Mass Transfer*, Vol. 46, No. 25, 2003, pp. 4935–4948. doi:10.1016/S0017-9310(03)00322-3

[15] Hibiki, T., and Ishii, M., "Interfacial Area Concentration of Bubbly Flow Systems," *Chemical Engineering Science*, Vol. 57, No. 18, 2002, pp. 3967–3977. doi:10.1016/S0009-2509(02)00263-4

[16] Lockhart, R. W., and Martinelli, R. C., "Proposed Correlation of Data for Isothermal Two-Phase Two-Component Flow in Pipes," *Chemical Engineering Progress*, Vol. 45, No. 1, 1949, pp. 39–48.

[17] Hibiki, T., Hogsett, S., and Ishii, M., "Local Measurements of Interfacial Area, Interfacial Velocity and Liquid Turbulence in Two-Phase Flow," *Nuclear Engineering and Design*, Vol. 184, No. 2-3, 1998, pp. 287–304. doi:10.1016/S0029-5493(98)00203-9

[18] Zuber, N., and Findlay, J. A., "Average Volumetric Concentration in Two-Phase Flow Systems," *Journal of Heat Transfer*, Vol. 87, No. 4, 1965, pp. 453–468.

[19] Hibiki, T., Situ, R., Mi, Y., and Ishii, M., "Modeling of Bubble-Layer Thickness for Formulation of One-Dimensional Interfacial Area Transport Equation in Subcooled Boiling Two-Phase Flow," *International Journal of Heat and Mass Transfer*, Vol. 46, No. 8, 2003, pp. 1409–1423. doi:10.1016/S0017-9310(02)00418-0

[20] Ishii, M., and Mishima, K., "Two-Fluid Model and Hydrodynamic Constitutive Relations," *Nuclear Engineering and Design*, Vol. 82, No. 2-3, 1984, pp. 107–126. doi:10.1016/0029-5493(84)90207-3

[21] Ishii, M., "One-Dimensional Drift-Flux Model and Constitutive Equations for Relative Motion Between Phases in Various Two-Phase Flow Regimes," Argonne National Lab. Rept. ANL-77-47, Argonne, IL, 1977.

R. Rangel
Associate Editor